NUMERICAL SIMULATION OF UNSTEADY CAVITATING FLOWS

Charles C.S. Song and Qiao Qin
St. Anthony Falls Laboratory, University of Minnesota
Mississippi River at 3rd Ave. SE, Minneapolis, MN 55414, USA

ABSTRACT

A previously developed simple numerical code, based on the Navier-Stokes equations of compressible fluid and a virtual single phase equation of state, has been applied to further demonstrate its capability to capture highly dynamic nature of cavitating flows about a two-dimensional NACA0015 hydrofoil. Computational time steps in the order of 10 microseconds were used to capture the detailed unsteady characteristics of bubble cavitation, bubble/cloud cavitation, sheet/cloud cavitation and super cavitation. The formation and collapse of cloud cavity, and the related generation and radiation of shock waves were visualized. The collapsing of cloud cavity is observed to be a highly unpredictable turbulent phenomenon, which most frequently breaks apart into a number of smaller pieces before collapsing. Only rarely it is found to collapse spherically as a whole. If the sheet cavity is long enough so that the cloud cavity can arrive at the tail of the foil before collapsing, refraction of negative pressure wave around the tail may cause cavitation to occur on the pressure side of the foil. The unsteadiness of natural super cavity is strongly influenced by the instability of the positive vortex sheet on the pressure side of the foil.

I. INTRODUCTION

Cavitating flows are highly turbulent and dynamic. Especially near the tail of a sheet cavity, generation and collapse of a cloud cavity, merging of trailing edge positive vortex sheet with cloud cavity, require a turbulent flow model that can simulate at least the largest scale eddies. To capture the radiation of pressure wave and its effect on the global flow field, it is necessary to include the compressibility effect of liquid phase as well as the gas phase. Song (1996) has shown that the compressibility effect may dominate the flow even if the Mach number is very small, provided that the flow changes rapidly enough. For this reason, a Large Eddy Simulation (LES) method based on the Navier –Stokes equations for compressible fluid was used as the base for the computational model. Strictly speaking the LES method assumes that the computational grids should be so small that the sub grid scale turbulence is isotropic. However, our experience indicates that the method can accurately simulate the primary and secondary eddies as long as the grids are sufficiently smaller than the size of eddy to be simulated.

A number of different approaches have been developed to deal with the equation of state for cavitating flows. Kunz et al (2000) developed a multiphase flow model in which the density of each component was assumed to be a constant. In other words, the flow was assumed to be incompressible even in the gas phase although an artificial compressibility method was used to make the numeric converges at each real time step. Kubota et al (1992) assumed that the fluid initially contains uniformly distributed small gas bubbles that will behave as described by the Rayleigh-Plesset equation in a changing pressure field. Song et al (1997, 1998) assumed that, for a natural cavitation, the liquid and gas phases are represented by a single continuous equation of state. This simple barotrotic flow model has been shown to produce results that agree very well with experimental data and observations, see Song and He (1998) and Arndt et al (2000). This model has been used to further study the detailed flow patterns over a NACA0015 hydrofoil at a constant angle of attack while the cavitation number is changed over a wide range. Various flow regimes including, bubble cavitation, bubble /cloud cavitation, sheet/cloud cavitation and super cavitation were produced and their characteristics studied.

II. GOVERNING EQUATIONS AND METHOD OF SOLUTION

The Navier-Stokes equations, including continuity and momentum equations are written in a conservative form as follows.

$$\frac{\partial U}{\partial t} + \nabla \bullet \vec{F} = S, \qquad \vec{F} = iE + jF + kG \tag{1}$$

where

$$U = [p, u, v, w]^T,\ E = \left[\rho a^2 u, \rho u^2 + p - \tau_{xx}, \rho uv - \tau_{xy}, \rho uw - \tau_{xz}\right]^T$$

$$F = \left[\rho a^2 v, \rho uv - \tau_{xy}, \rho v^2 + p - \tau_{yy}, \rho vw - \tau_{yz}\right]^T$$

$$G = \left[\rho a^2 w, \rho uw - \tau_{xz}, \rho vw - \tau_{yz}, \rho w^2 + p - \tau_{zz}\right]^T,\ S = \left[\rho \vec{V} \bullet \nabla a^2, 0, 0, 0\right]^T$$

In the above equations, *a* is the speed of sound defined as

$$\frac{\partial p}{\partial \rho} = a^2 \tag{2}$$

τ_{xy} Is shear stress tenser containing laminar and turbulent stresses. For the turbulent shear stress, Smagorinsky's (1963) SGS turbulence model is used.

Water is assumed to vaporize or condensate reversibly at a critical pressure p_c, which is usually taken as the vapor pressure. For the liquid phase, the equation of state is

$$p - p_o = a_o^2 (\rho - \rho_o) \tag{3}$$

where the subscript o represent a reference condition. For the gas phase, the following equations are assumed.

$$p = \sum_{i=0}^{5} A_i \rho^i, \qquad \varepsilon \le p \le p_c \tag{4}$$

$$p = B\rho, \qquad 0 \le p \le \varepsilon \tag{5}$$

The coefficients in the above equations are so determined that the equations are continuous but have a sharp gradient below the critical pressure, p_c, to simulate a sharp change in density when cavitation occurs. ε is a small number so chosen to make density equal to zero when pressure is zero.

To apply a finite volume method, Eq. 1 is first averaged over an arbitrary finite volume to obtain

$$\frac{\partial \overline{U}}{\partial t} + \frac{1}{\Delta V} \iint_{\Delta A} \vec{F} \bullet \vec{n} dA = \overline{S} \tag{6}$$

In the above equation, ΔV is the finite volume, ΔA is the surface surrounding the finite volume and the superscript bar represents average over the finite volume. Note that the divergence theory has been applied to convert the volume integral to the surface integral. Consistent with the finite volume approach, the SGS turbulence model represents the effect of turbulence of size smaller than the finite volume. MacCormack's (1969) predictor-corrector method, nominally second order accurate, is adopted. This is an explicit method requiring the time step to be small enough to satisfy the CFL stability criterion.

The numerical model is very robust and the computation can start with any initial condition. For an example, a zero flow condition may be assumed to start the computation and let the flow establishes itself before necessary data are recorded. Then, the cavitation number may be changed by changing the ambient pressure and continue the simulation for a different flow condition. When a new condition is given in the middle of computation, a new fully developed condition will be achieved after a brief transient period without any numerical problem. Although it may be desirable to use a non-reflective boundary condition, especially in dealing with acoustics, the following upstream boundary condition is found to be sufficiently accurate for hydrodynamic aspect of the flow.

$$u = U, \partial u/\partial x = \partial v/\partial x = \partial w/\partial x = \partial p/\partial x = 0 \tag{7}$$

For the downstream boundary, the following condition is applied.

$$\overline{p} = p_o, \partial u/\partial x = \partial v/\partial x = \partial w/\partial x = \partial p/\partial x \tag{8}$$

In the above equation, the superscript bar indicates the value averaged over the downstream end section. Note that it is not possible to fix the pressure on the entire downstream end section because the flow is unsteady and three-dimensional. On the imaginary side boundary, the full slip condition is used. On the real solid boundary of the hydrofoil, a partial slip condition derived from the concept of wall function is used to account for the effect of thin viscous boundary layer.

The most important parameters considered are the angle of attack α and the cavitation number σ defined as

$$\sigma = \frac{p_o - p_c}{0.5\rho U^2} \tag{9}$$

III. COMPUTATIONAL RESULTS

Only two-dimensional aspects of the cavitating flow were simulated by taking only three grids in the span wise direction. The angle of attack and the Reynolds number were kept equal to 8 degrees and 10^5, respectively, and the cavitation number was varied over a range of 2.5 – 0.05 in order to simulate various flow regimes. The results to be presented here were obtained with a grid system. No free stream turbulence was given so that the turbulence was essentially cavitation generated.

3.1 Noncavitating Flow

To serve as a reference condition for the Cavitating flow to follow, a noncavitating flow condition was computed by setting $\sigma = 2.5$. When the cavitation number is above the critical value, there is no cavitation and the boundary layer is very thin and fully attached. This is most clearly observable with the vorticity field shown in Fig. 1 (b). The corresponding pressure field is shown in Fig. 1 (a). The well known vortex street in the wake is also clearly shown in both figures. Because of the wake vortex street, the lift coefficient as shown in Fig. 2 oscillates at the Strouhal number based on the cord length of 5.6 and the peak to peak amplitude of approximately 0.2.

3.2 Bubble Cavitation

It has been reported by Arndt et al (2000) that, at slightly below the critical cavitation number, the "bubble/patch cavitation" first appears. But, patch cavitation is a three-dimensional phenomenon so that only bubble cavitation appears with current simulation. It is a periodical phenomenon whose Strouhal number based on the cord length is approximately equal to 0.1. A cavitation bubble first occurs at the point of minimum pressure near the nose when the lift coefficient is maximum. The bubble cavity, which is also

an eddy, slides down the foil and the lift decreases to a minimum when it arrives at the tail of the foil. The lift starts to increase again as the eddy moves away in the wake. A new bubble cavity occurs when the lift increases to a maximum again and the process repeat itself. For more detailed flow pattern and pressure and lift oscillation, reference is made to Arndt et al.

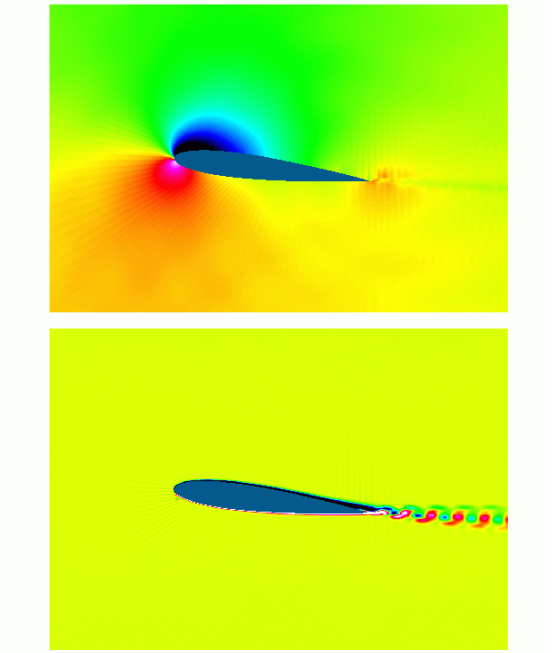

Fig. 1 Pressure (a) and vortcity (b) field of noncavitating Flow, $\sigma = 2.5$

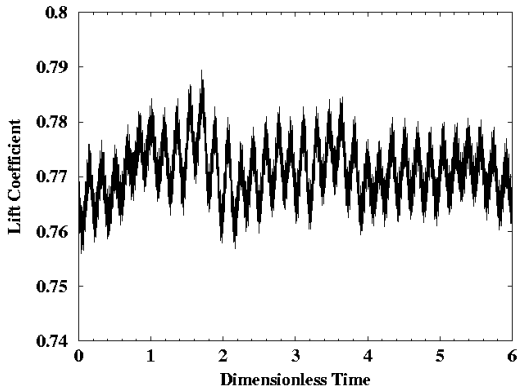

Fig. 2 Lift coefficient as a function of time, Noncavitating flow

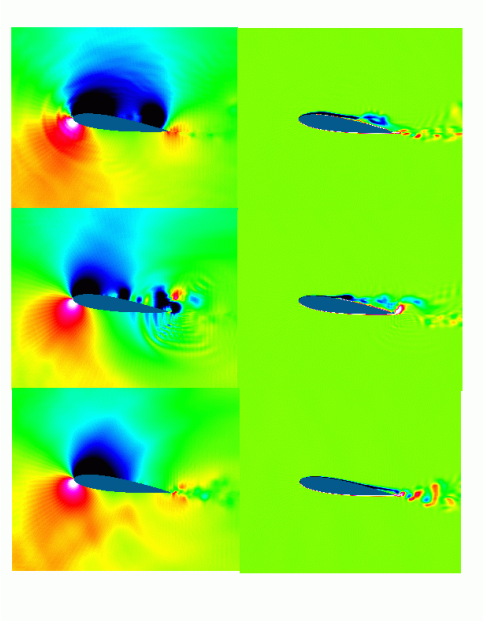

Fig. 3 Pressure (a-c) and vorticity (d-f) fields of bubble/cloud cavitation, $\sigma = 2.0$

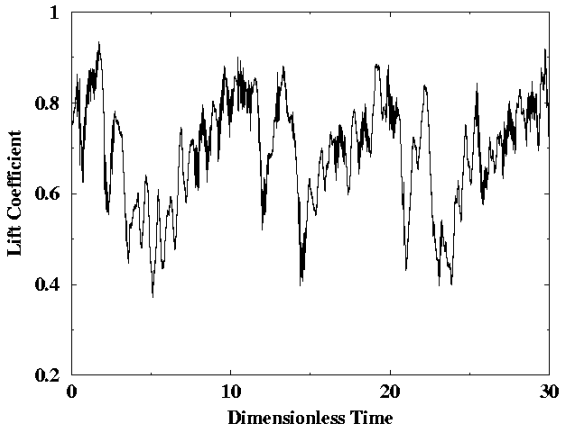

Fig. 4 Lift coefficient as a function of time, $\sigma = 2.0$

3.3 Bubble/Cloud Cavitation

Pure bubble cavitation may change to a less stable bubble/Cloud cavitation with a small change in the cavitation number. As illustrated in Fig. 3, at $\sigma = 2.0$ a clod cavity may follow a small bubble near the time of maximum lift. When the cloud cavity collapses near the trailing edge the lift drops to a minimum. The small bubble is less dynamic and behaves like the bubble cavity described before. As indicated by Fig. 4, the lift coefficient oscillates fairly regularly at Strouhal number approximately equal to 0.1. The difference between this flow regime and the purely bubble cavity regime is that there is a severe lift fluctuation associated with the collapse of each cloud cavity.

3.4 Sheet/Cloud Cavitation

This is a widely recognized and the most dynamic flow regime related to partial cavitation. Fairly extensive discussions regarding this flow regime were given by Arndt et al (2000). Some additional interesting and newly discovered phenomena will be presented here.

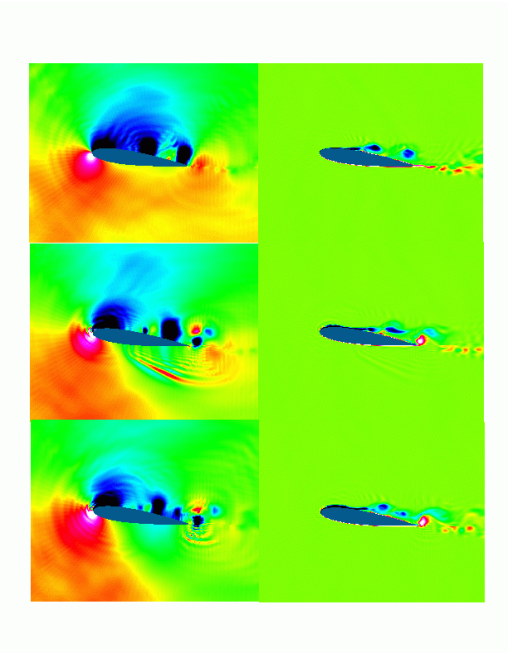

Fig. 5 Pressure (a-c) and vorticity (d-f) of sheet/cloud cavity, $\sigma = 1.5$

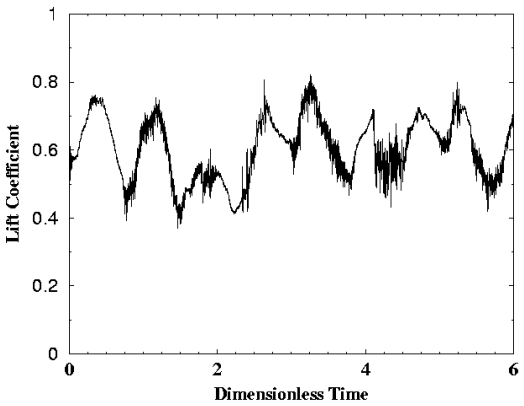

Fig. 6 Lift coefficient as function of time, $\sigma = 1.5$

Fig. 5 shows some typical instantaneous vortivity fields and the corresponding pressure field for $\sigma = 1.5$ case. Sheet cavity is quite short and it breaks up by reentrant jet to form a cloud cavity at about 1/3 cord. The cloud cavity collapses at near ¾ cord to generate strong shock wave. Fig. 6 shows the variation of lift coefficient with time. The average Strouhal number of this process is about 1.5 but, in reality, it is inherently a turbulent phenomenon with significant degree of randomness. In most cases a cloud cavity breaks up and collapses into more than one piece as shown in Fig. 5. Very rarely will it collapse spherically as indicated by Reisman et al (1998). By assuming a spherical cloud consisting of uniform size small bubbles, they concluded that the cavity will collapse and rebound while maintaining spherical shape. We did find a case where the cloud cavity collapses in nearly spherical form, creating a shock wave first radiating inward and then radiate outward as shown in Fig. 7. Note that, by assuming water to be compressible, we are able to capture the outward radiation of the shock wave.

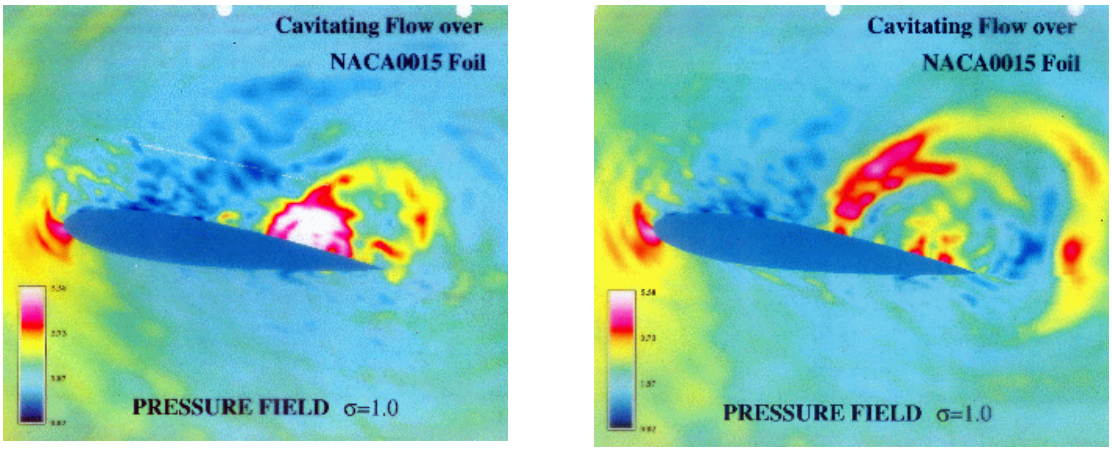

Fig. 7 Instantaneous pressure fields due to nearly spherical collapsing of cloud cavity

Fig. 8 shows typical instantaneous pressure and vorticity fields when $\sigma = 1.0$. In this case the sheet cavity approaches ¾ cord before broken off by the reentrant jet. The vorticity field clearly shows that the jet, having positive vorticity indicated by red, breaks up the sheet cavity and raps around the cloud cavity. An interesting phenomenon is that, because this low pressure cloud arrives at the trailing edge before it has time to collapse, rarefaction waves are emitted and deflected around the trailing edge, which travels upstream on the pressure side. This rarefaction wave is responsible for the occurrence of unsteady cavitation on the pressure side of the foil, which has been observed experimentally and numerically. This is another example showing the importance of compressibility and unsteadiness in simulating cavitating flows. The time dependent lift coefficient is plotted in Fig. 9. The dominant Strouhal number is 0.5.

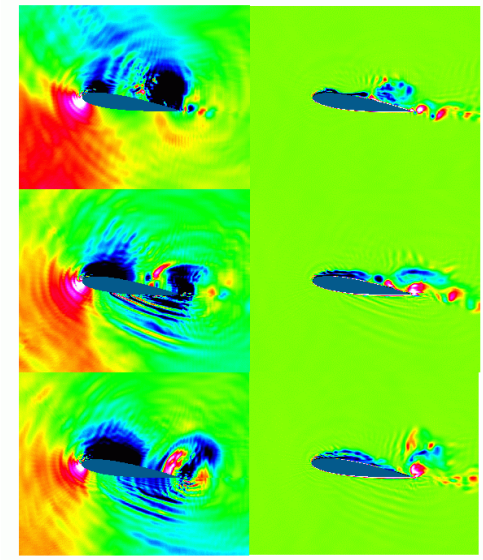

Fig. 8 Pressure (a-c) and vorticity (d-f) of Sheet/cloud cavity, $\sigma = 1.0$

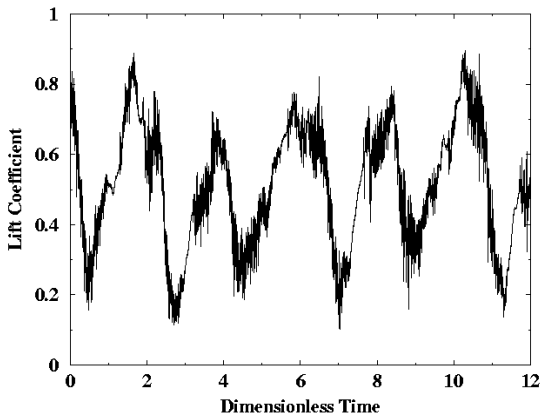

Fig. 9 Lift coefficient as a function of time, $\sigma = 1.0$

Another interesting phenomenon to be noted is the radiation of strong pressure waves from the nose of the foil when the flow is highly unsteady. We suspect this is due to shifting stagnation point, but no detailed investigation on the mechanism of this noise source has been carried out.

3.5 Super Cavitation

Fig. 10 shows typical instantaneous vorticity and pressure fields for the case $\sigma = 0.05$. The corresponding lift coefficient as a function of time is shown in Fig. 11. The main mechanism of flow unsteadiness appears to be the instability of positive vortex sheet produced by the boundary layer on the pressure side of the foil. The positive vortex sheet indicated by red color roles up to form a vortex street and breaks the cavity near its tail. The broken away free cavity also collapses to produce pressure waves in much the same way that was observed with partial cavitation.

Somewhat unexpected phenomenon is the existence of many small pieces of high pressure zones near the cavity detachment point as shown in Fig. 10. It appears that the pressure waves emitted from the nose may be strong enough to make local cavity collapsing. More detailed studies, experimental and numerical, are necessary to understand this phenomenon.

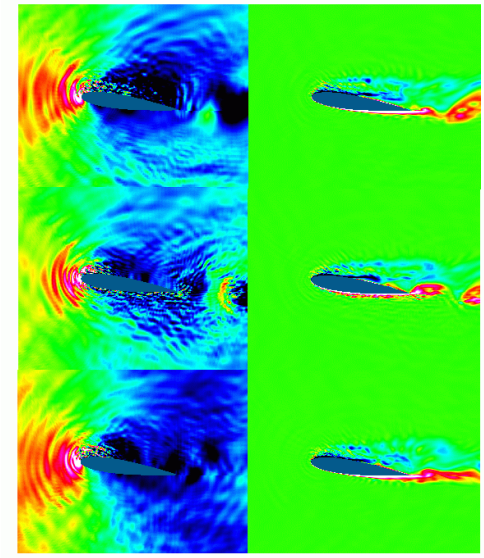

Fig. 10 Pressure (a-c) and vorticity (d-f) fields of Super cvitation, $\sigma = 0.05$

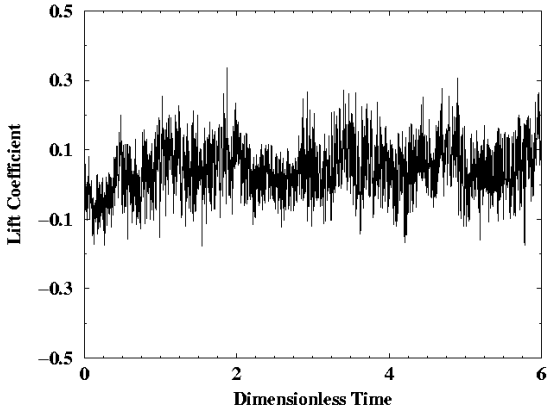

Fig. 11 Lift coefficient as a function of time, $\sigma = 0.05$

IV. CONCLUSIONS

A three-dimensional unsteady compressible turbulent flow model plus a virtual single-phase equation of state has been used to simulate Cavitating and non-cavitating flow about a two-dimensional NACA 0015 hydrofoil. By fixing the attach angle to 8 degrees and Reynolds number to 10^5, but varying the cavitation number, four different unsteady cavitating flow regimes are identified and studied. The sheet/cloud cavity regime related to partial cavitation is the most dynamic of all. Shock waves generated by collapsing cloud cavity were found most frequently collapses into more than one piece. Only rarely one may capture a cloud cavity collapsing in nearly spherical form. A cloud cavity generated by a long sheet cavity may emit

rarefaction waves before collapsing to cause cavitation on the pressure side. Within a small cavitation number range, cloud cavitation may also coexist, alternatively, with bubble cavity. In all the flow conditions simulated, the lift coefficient oscillates with recognizable characteristic frequencies.

Even a super cavity is unsteady and collapsing cavity generates relatively weaker shock wave. In this case the main mechanism driving the flow unsteadiness appears to be that of the vortex sheet instability. Strong pressure waves are emitted from the nose of the foil when Cavitating. The mechanism of this phenomenon deserves further study.

ACKNOWLEDMENT

This study has been partially supported by the Office of Naval Research and the National Science Foundation. The computer time has been provided by the Minnesota Supercomputer Institute of the University of Minnesota.

REFERENCES

Arndt, R.E.A., Song, C.C.S., Kjeldsen, M., He, J. and Keller, A., "Instability of Partial cavitation: A Numerical/Experimental Approach," *23 rd Symposium on Naval Hydrodynamics*, Sept., Rouen, France.

Kubota, A., Kato. H. and Yamaguchi, H.. 1992, "A New Modeling of Cavitating Flows: a Numerical Study of Unsteady Cavitation on a Hydrofoil Section," *Journal of fluid Mechanics*, Vol. 249, pp. 59-96.

Kunz, R.F., Boger, D.A., Stinebring, D.R., Chyczewski, T.S., Lindau, J.W., Gibeling, H.J., Venkateswaran, S. and Govindan, T.R., 2000, "A Preconditioned Navier-Stokes Method for Two-Phase Flows with Application to Cavitation Prediction," *Computers & Fluids*, 29, pp. 849-875.

MacCormack, R.W., 1969, "The Effect of Viscosity in Hypervelocity Impact Cratering," *AIAA Paper 69 -354*,Cincinati, Ohio.

Reisman, G.E., Wang, Y.C. and Brennen, C.E., 1998, "Observation of Shock Waves in Cloud Cavitation," *J. Fluid Mech*, Vol. 355, pp.255-283.

Smagorinsky, J., 1963, "General Circulation Experiments with the Primitive Equations," *Monthly Weather Review*, Vol. 91, No. 3, pp. 99-164.

Song, C.C.S., 1996, "Compressibility Boundary Layer Theory and its Significance in Computational Hydrodynamics," *Journal of Hydrodynamics*, Series B, Vol. 8, No. 2, pp. 92-101.

Song, C.C.S., He, J., Zhou, F. and Wang, G., 1997, "Numerical Simulation of Caviling and Non-Cavitating Flows Over a Hydrofoil," *SAFL Project Report No. 402*.

Song, C.C.S and He, J., 1998, "Numerical Simulation of Cavitating Flows by Single-phase Flow Approach," *3rd International Symposium on Cavitation*, Grenoble, France, pp. 295-3000.